Timing and *PT* Evolution of Whiteschist Metamorphism in the Lufilian Arc—Zambezi Belt Orogen (Zambia): Implications for the Assembly of Gondwana

Author(s): Timm John, Volker Schenk, Klaus Mezger and Francis Tembo

Source: *The Journal of Geology*, Vol. 112, No. 1 (January 2004), pp. 71-90
Published by: The University of Chicago Press
Stable URL: http://www.jstor.org/stable/10.1086/379693
Accessed: 20-09-2016 05:38 UTC

Timing and *PT* Evolution of Whiteschist Metamorphism in the Lufilian Arc–Zambezi Belt Orogen (Zambia): Implications for the Assembly of Gondwana

Timm John,[1,2] *Volker Schenk, Klaus Mezger,*[2] *and Francis Tembo*[3]

Institut für Geowissenschaften, Universität Kiel, Olshausenstrasse 40, 24098 Kiel, Germany
(e-mail: tj@min.uni-kiel.de)

ABSTRACT

One of the world's most extensive occurrences of whiteschists (talc-kyanite schists) is located in south central Africa with several exposures along a ca. 700 km northwest-southeast striking zone. The metamorphic evolution and age relations of whiteschists and associated rocks from four localities, three in the Lufilian Arc and one in the Zambezi Belt, were investigated. In the Lufilian Arc whiteschists, associated garnet-amphibolites and biotite-kyanite-garnet gneisses record peak metamorphic conditions of about 750° ± 25°C at 13 ± 1 kbar. Whiteschists, associated anthophyllite-cordierite-kyanite gneisses, and garnet-staurolite-kyanite schists from the Zambezi Belt indicate peak metamorphic conditions of about 700° ± 25°C at 10 ± 1 kbar. Mineral reaction textures imply a metamorphic evolution along clockwise *PT* paths with peak metamorphism culminating at high-pressure amphibolite facies conditions. The shapes of the *PT* paths are interpreted to result from crustal thickening. On the basis of these interpretations and a concordant monazite age of 529 ± 2 Ma for a biotite-kyanite-garnet gneiss combined with $^{207}Pb/^{235}U$ ages of 531 to 532 ± 2 Ma from monazites from whiteschists, we concluded that the crustal thickening event affected the entire Lufilian Arc–Zambezi Belt orogen almost simultaneously. Whiteschist formation was related to the final continental collision between the Congo and the Kalahari cratons at ca. 530 Ma during the assembly of Gondwana, which followed the subduction of oceanic lithosphere and eclogite formation at about 600 Ma.

Online enhancements: appendix, references cited, tables.

Introduction

The Pan-African orogenies that developed during the assembly of the supercontinent Gondwana between 750 and 500 Ma (Condie 2002) represent the last major orogenic cycle that formed and reworked the continental crust of Africa. Determining the relationship between the large continental shields of the Kalahari and the Congo cratons allows for an understanding of the assembly of Gondwana as well as the geodynamic setting of the final formation and reworking of the African continental crust. A key location for the investigation of this relationship during the crucial time period is the prominent east-west striking Pan-African transcontinental belt (fig. 1), which separates these two cratons (e.g., Porada 1989).

A formerly widely accepted hypothesis held that the Congo and the Kalahari cratons formed one continuous shield before the Gondwana assembly started and that there was only minor rifting in between (e.g., Hanson et al. 1994). However, in recent years evidence for a different scenario has been found. For example, Porada and Berhorst (2000) proposed that rifting started at ca. 880 Ma and separated the Congo-Tanzania plate probably from the Angola-Kalahari plate, leading to the formation of a passive continental margin on the southern side of the Congo craton. Geochemical data and *PT* estimates from Zambian eclogites (Zambezi Belt) give evidence for subduction of oceanic crust at ca. 600 Ma (John et al. 2003). However, not much is known about the final continental collision that caused the

Manuscript received November 1, 2002; accepted April 30, 2003.

[1] Author for correspondence.
[2] Institute für Mineralogie, Universität Münster, Corrensstrasse 24, 48149 Münster, Germany.
[3] School of Mines, University of Zambia, P.O. Box 32379, Lusaka, Zambia.

[The Journal of Geology, 2004, volume 112, p. 71–90] 0022-1376/2004/11201-0005$15.00

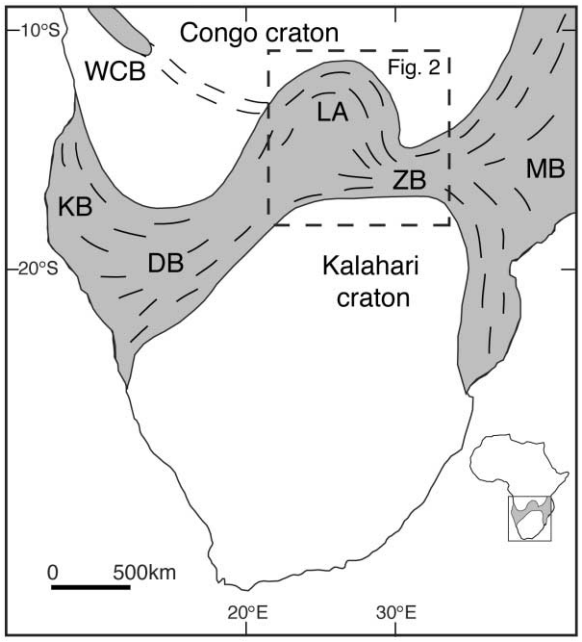

Figure 1. Pan-African Belts in central southern Africa and their general strike (*gray*). *WCB* = West Congo Belt; *KB* = Kaoko Belt; *DB* = Damara Belt; *LA* = Lufilian Arc; *ZB* = Zambezi Belt; *MB* = Moçambique Belt.

crustal thickening within this transcontinental Pan-African belt.

Whiteschists (talc-kyanite schists) are low-temperature/high-pressure rocks that, as potential subduction- and collision-related rocks (Schreyer 1973), may provide additional information about orogenic evolution. Whiteschists typically are found in Alpine-type orogens (e.g., Western Alps and Hindu Kush; Schreyer and Abraham 1976; Chopin 1984) and are usually interpreted as being of metasomatic origin. Metasomatism may occur before (e.g., Pawlig and Baumgartner 2001) or during metamorphism (e.g., Johnson and Oliver 2002), while the precursor rocks are in most cases of felsic (e.g., Pawlig and Baumgartner 2001) or, rarely, of mafic or sedimentary origin (e.g., Schreyer and Abraham 1976; Johnson and Oliver 2002). The stability field of the talc-kyanite assemblage is restricted to temperatures between ca. 600° and 800°C and pressures from ca. 6 kbar up to conditions of the ultrahighpressure metamorphism (>30 kbar) (e.g., Chopin 1984; Massonne 1989), thus whiteschists are formed during subduction or crustal thickening under a low geothermal gradient. Zambia hosts one of the most extensive occurrences of whiteschists in the world (Vrána and Barr 1972; Schreyer 1977). In southern Africa, one additional whiteschist occurrence is known from northern Zimbabwe (Johnson and Oliver 1998, 2002) within the spatial extension of the Zambian occurrences (*C* in fig. 2). For the reconstruction of the geological evolution of the Lufilian Arc–Zambezi Belt whiteschists and associated rocks (metapelites and anthophyllite-cordierite-kyanite gneisses), four whiteschist localities were chosen for petrological and geochronological studies, three within the Lufilian Arc and one within the Zambezi Belt. Mineral-chemical and textural investigations in combination with quantitative geothermobarometry have been used to reconstruct the metamorphic evolution of the high-pressure rocks. The results are used to identify the geodynamic situation at the time of metamorphism. Peak metamorphic conditions have been dated with monazites, while cooling has been dated with whole rock-mica Rb-Sr ages. In addition, basement rocks to whiteschists in the Lufilian Arc have been dated with zircons.

Regional Geology

The Precambrian crust of Zambia has been affected by three major orogenic events (fig. 2). Paleoproterozoic crust (ca. 2.0–1.8 Ga) occurs in the northeast of Zambia in the Bangweulu Block (Andersen and Unrug 1984), while the Mesoproterozoic (ca. 1.3–1.0 Ga) northeast-southwest striking Irumide Belt and Choma-Kalomo Block occur in south and east Zambia (e.g., Hanson et al. 1988). In central Zambia, the Mesoproterozoic units are crosscut by the Pan-African Lufilian Arc and Zambezi Belt (fig. 1), and both have a general east-west trend (e.g., Porada 1989). The two younger orogens are thought to be related to two major supercontinent-forming events, the Mesoproterozoic (ca. 1.3–1.0 Ga) Rodinia assembly (e.g., Dalziel 1992; Porada and Berhorst 2000) and the Late Proterozoic to Cambrian (ca. 750–500 Ma) Gondwana assembly (e.g., Porada 1989; Unrug 1996).

A continuous transition from the Zambezi Belt into the Moçambique Belt is postulated for the region northeast of the Kalahari craton (Johnson and Vail 1965). The northwestern end of the Zambezi Belt is defined by the Mwembeshi Shear Zone (MSZ), which separates the Zambezi Belt from the Lufilian Arc (e.g., Porada 1989; fig. 2). According to Porada and Berhorst (2000), the importance of this dislocation zone as a dividing line between the Lufilian Arc and the Zambezi Belt is debatable. The Lufilian Arc continues toward the west into the Damara Belt, or into the West Congo Belt (Porada and Berhorst 2000; Key et al 2001). The presence

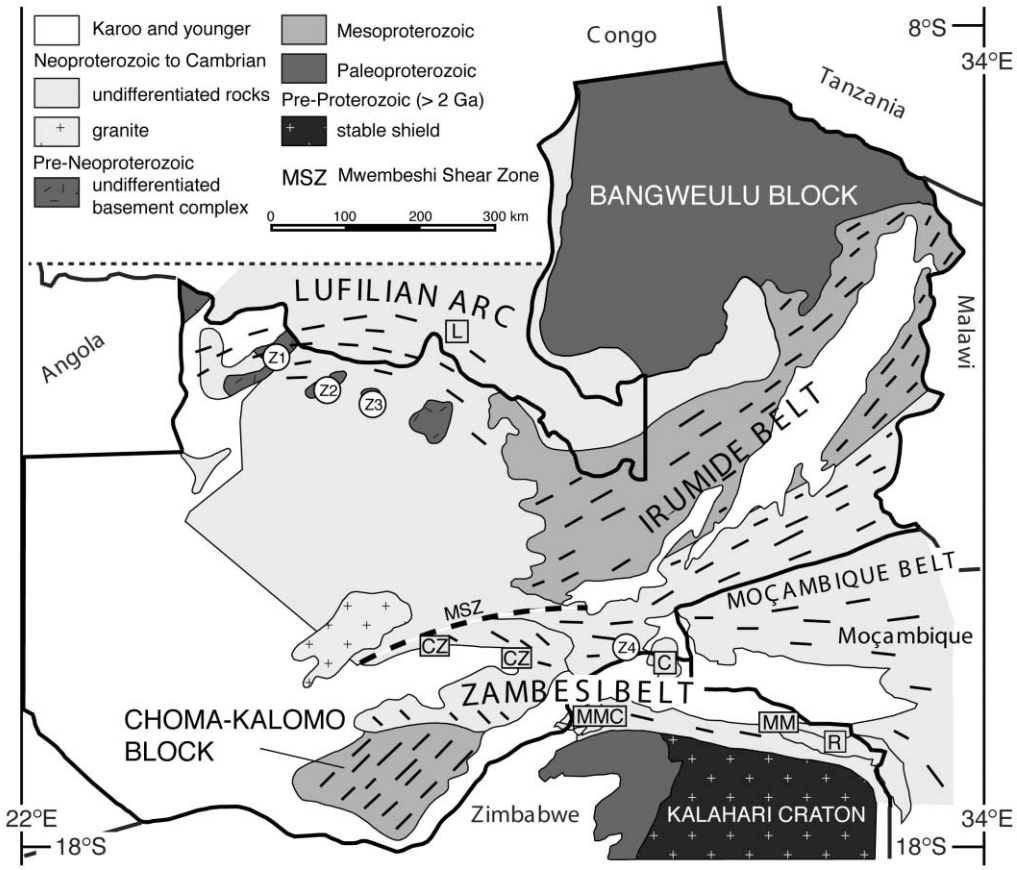

Figure 2. Structural provinces of Zambia, Northern Zimbabwe, and Western Moçambique, modified after Sikatali et al. (1994) and Hanson et al. (1994). *Z1–Z4* = investigated areas: *Z1* = Kabompo Dome, *Z2* = Mwombezhi Dome, *Z3* = Solwezi Dome, *Z4* = Chowe River (Chongwe River area). *L* = Lwiswishi; *CZ* = central Zambia; *MMC* = Makuti Metamorphic Complex; *C* = Chewore Inliers; *MM* = Mavuradonha Mountains; *R* = Rushinga area. The northern edge of the Kalahari craton is shown, while the Congo craton is north of the figure. Thin lines indicate geological boundaries; thick lines indicate political borders.

of reworked older basement components is an important feature of the southern Zambezi Belt (Goscombe et al. 1998). In the Lufilian Arc, basement rocks are less extensively reworked and are mainly exposed in the Domes Region, where the basement is overlain by rocks of the Neoproterozoic to Cambrian Katanga Supergroup (ca. 870–530 Ma; Porada and Berhorst 2000; H. Porada, pers. comm., 2003). Rb-Sr whole rock and U-Pb zircon SHRIMP ages (Cahen et al. 1984; Rainaud et al. 1999) yielded ages between 2.0 and 1.8 Ga for the basement rocks at the eastern margin of the Lufilian Arc. In contrast, a whole rock Rb-Sr isochron using samples from the basement of the Domes Region points to a Mesoproterozoic age of ca. 1.2 Ga (Cosi et al. 1992).

In the central Zambezi Belt, Mesoproterozoic crustal fragments are located in the Chewore Inliers (fig. 2). Here, crystallization ages approximately 1070 to 1080 Ma were determined and a low-*P*/high-*T* metamorphic event with a minimum age of about 945 Ma and a high-*P*/medium-*T* metamorphic event at ca. 526 Ma has been dated with the SHRIMP technique on zircon (Goscombe et al. 2000). In addition, for the Rushinga area in northeast Zimbabwe (fig. 2) two distinguishable metamorphic events are reported. A high-pressure granulite facies migmatization event between 870 and 850 Ma and an amphibolite facies event at ca. 535 Ma are constrained by zircon and titanite U-Pb ages and Ar-Ar amphibole ages (Vinyu et al. 1999). Based on geochemical and structural studies, an extensional regime with intrusions of peralkaline rocks at the time of the first metamorphism has been postulated for the Rushinga area (Dirks et al. 1998; Vinyu et al. 1999). Furthermore, granites and volcanic rocks with ages ranging from 880 to 840 Ma

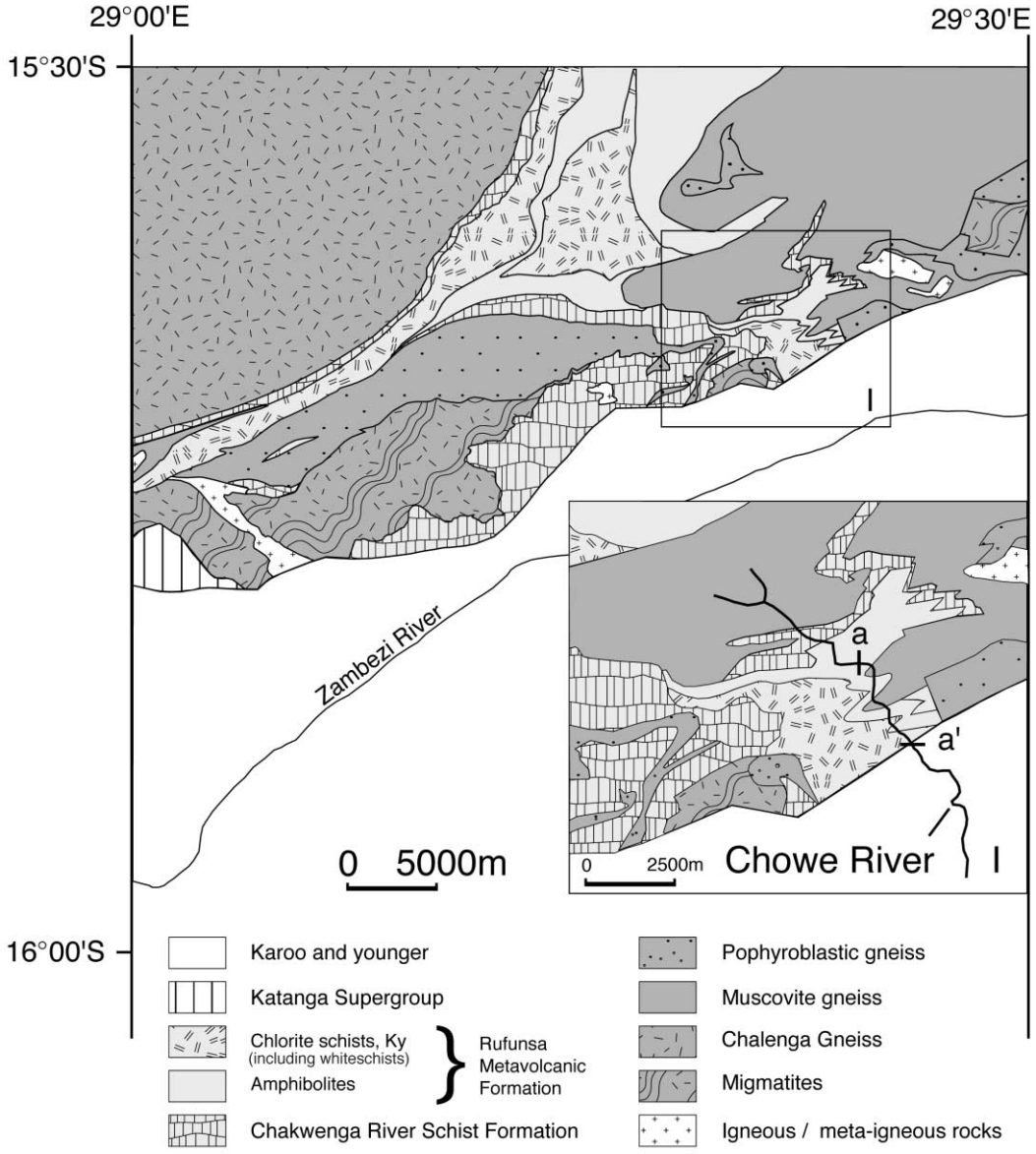

Figure 3. Simplified geological map of the Chongwe River Area, after Barr (1997). Inset map shows the sampled river section (*a*–*a*′).

are widespread within the Lufilian Arc–Zambezi Belt and are interpreted as indicators of extension (references in Porada and Berhorst 2000).

Porada and Berhorst (2000) proposed that during rifting, a passive continental margin formed along the southern edge of the Congo craton. Geochemical investigations of gabbros and metagabbros from the Lufilian Arc were interpreted as an indication that the rifting probably did not significantly overstep a continental stage (Tembo et al. 1999), but geochemical data obtained from eclogites and gabbros of central Zambia give evidence that they were formed at an oceanic spreading center and that they are relics of a subducted Neoproterozoic oceanic crust. The time of eclogite formation is constrained by Sm-Nd garnet whole rock ages of ca. 600 Ma (John et al. 2003).

Sample Areas

Zambezi Belt: Chowe River Section. Whiteschist in the Zambezi Belt occurs close to the Chowe River (fig. 3; *Z4* in fig. 2) and was first described by Vrána and Barr (1972). Following Barr (mapped in

1970, published 1997), the migmatic and leucocratic Chalenga Gneiss, porphyroblastic two-feldspar and muscovite gneisses, and migmatites form the basement in this area (fig. 3). The basement is locally overlain by the Mesoproterozoic Muva Supergroup, composed of the Rufunsa Metavolcanic Formation and the Chakwenga River Schist Formation. The Rufunsa Metavolcanic Formation consists of amphibolites and kyanite-bearing chlorite schists that include the investigated metapelites, whiteschists, and anthophyllite-cordierite-kyanite gneisses. The Chakwenga River Schist Formation consists of biotite-plagioclase schists, amphibolites, and calc-silicate rocks (fig. 3). A detailed description of the sampled outcrops, including the latitudes and longitudes, are given in table B1 in the online edition of the *The Journal of Geology*.

Lufilian Arc: Domes Region. The investigated whiteschist occurrences within the Lufilian Arc are all situated in the Domes region. Each of the localities belongs to a different dome (i.e., the Kabompo, the Mwombezhi, and the Solwezi Dome; fig. 4). The domes consist mainly of basement rocks unconformably overlain at their margins by rocks of the Neoproterozoic Katanga Supergroup. Rocks of the Mesoproterozoic Muva Supergroup are only found along the eastern margin of the Lufilian Arc. No significant differences in the lithologies among the domes have been observed (Cosi et al. 1992). The contacts between the rocks of the lower units of the Katanga Supergroup and the basement rocks of the domes are not clearly defined and are usually interpreted as sheared. The basement consists of biotite gneisses, schistose gneisses, and rare migmatites. The Katanga Supergroup within and around the domes mainly consists of the lower units of the Roan Group with Mg-rich quartzites, mica schists, metapelites, and amphibolites. Whiteschists commonly occur close to the contact between basement and Roan Group and are thus interpreted to belong to the lowest unit of the Roan Group. The whiteschists are mainly exposed along the margins of the domes, but rare outcrops exist within the domes. The whiteschists were either sampled at the rim (Solwezi Dome) or within a dome (Kabompo and Mwombezhi Domes). Additionally, biotite-kyanite-garnet gneisses and garnet amphibolites were sampled within the Solwezi Dome. Basement rocks were sampled from the Kabompo and the Solwezi Dome (fig. 4). A detailed description of the sampled outcrops, including the latitudes and longitudes, are given in table B1.

Petrography and Mineral Chemistry

Mineral assemblages are given in table 1 and representative microprobe analyses are given in tables B2–B12 in the online edition of *The Journal of Geology*. Mineral abbreviations are from Kretz (1983). For details of the microprobe analyses, see appendix A in the online edition of *The Journal of Geology*.

Zambezi Belt: Whiteschists and Related Chowe River Rocks. The whiteschists of the Chowe river occur in two varieties. The grayish white variety (whiteschist sensu stricto) contains the assemblage talc-kyanite-cordierite-quartz-chlorite-hematite-tourmaline ± albite ± phlogopite and rutile. Kyanite may be centimeter sized, while all other minerals are mainly in the millimeter range. The contact between talc and kyanite is characterized by a reaction rim of cordierite (fig. 5*a*). Cordierite is completely altered to pinite with low X_{Fe} values of 0.07 to 0.10. Talc (X_{Fe} ~0.03) has a high alumina content with Al ≈ 0.20 to 0.40 per formula unit (pfu). Tourmaline is Fe-rich dravite. Sample 8HC 234 (described by Vrána and Barr 1972; reanalyzed for this study) displays an equilibrium mineral assemblage of talc-quartz-albite(Ab_{99})-kyanite. This assemblage, which occurs also as inclusions in kyanite, is interpreted to represent the equilibrium assemblage during peak metamorphic conditions. Phlogopite occurs only in the matrix and is related to the retrograde evolution of this rock. The more greenish whiteschist variety contains less or no talc but more Mg-chlorite (X_{Fe} = 0.03). In some samples kyanite is surrounded by sericite, whereas in other samples kyanite is completely replaced by a fine-grained intergrowth of sericite, talc, and quartz.

The mineral assemblages of the anthophyllite-cordierite-kyanite gneiss are anthophyllite-hornblende-quartz-kyanite-cordierite ± talc ± mg-chlorite ± phlogopite. Staurolite may occur as inclusion in both amphiboles and quartz (fig. 5*b*). The amphiboles are centimeter sized, while all other minerals display grain sizes in the millimeter range. Cordierite may also form more than 10-cm large crystals segregated along cracks and in veins. Unzoned anthophyllite (X_{Fe} = 0.17 to 0.21) and tschermakitic hornblende (X_{Fe} = 0.17 to 0.20) are intergrown and constitute up to 70% of the rock. Staurolite (X_{Fe} = 0.61 to 0.62) inclusions have very low ZnO contents (≤0.1 wt%). Kyanite is closely associated with orthoamphibole and always shows a reaction rim of cordierite (X_{Fe} = 0.11 to 0.12; Na_2O ≤0.3 wt%; fig. 5*c*). Quartz is a matrix mineral but is also common as inclusions in poikiloblastic amphibole and in intergrowths with cordierite. Locally, retrograde talc forms small flakes along rims

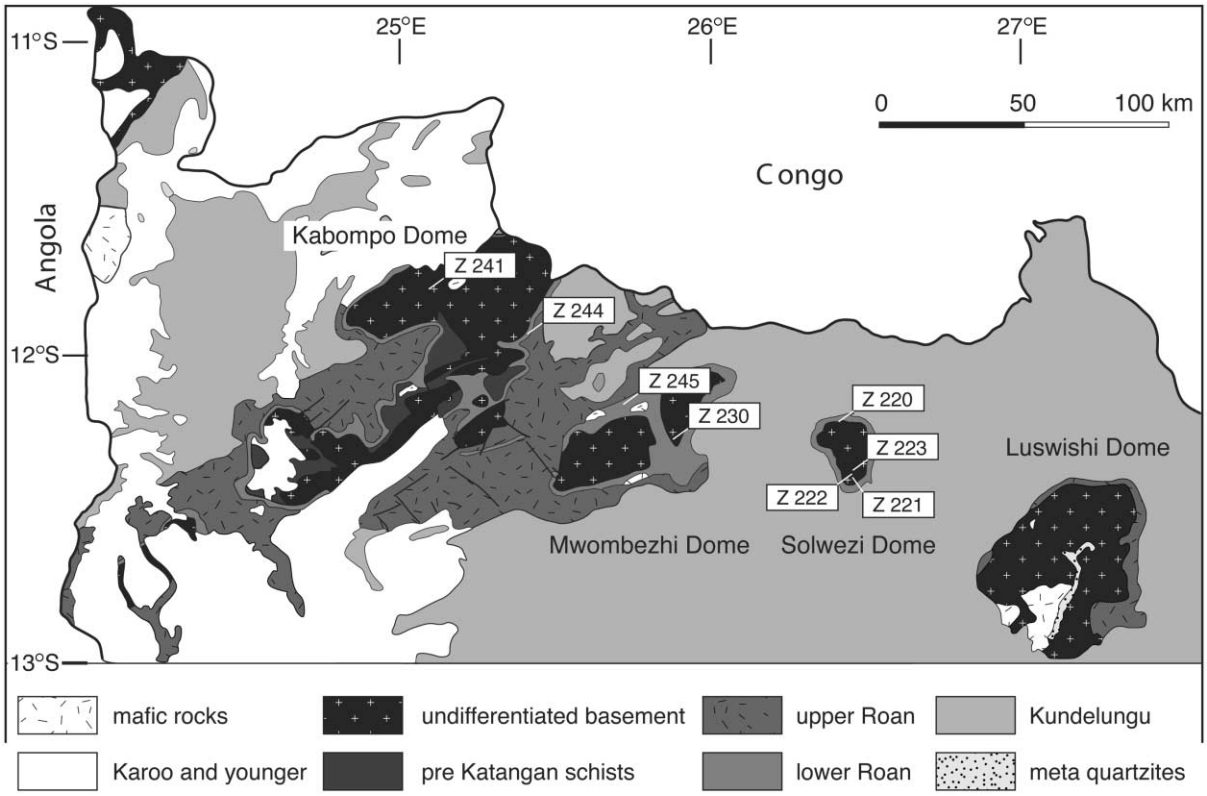

Figure 4. Sample locations in simplified geological map of the Domes Region, after Thieme and Johnson (1977). Thin lines indicate geologic boundaries; thick lines indicate political borders.

of anthophyllite. Common accessories are Fe-rich dravite, phlogopite, ilmenite, and rutile.

Metapelites are rare in the river section. They have the mineral assemblage garnet-quartz-white mica-plagioclase-kyanite-staurolite-chlorite ± biotite ± chloritoid. Grain sizes are in the millimeter range except for garnet and the rare staurolite, which reach centimeter size. Garnet shows sigmoidal inclusion trails of kyanite, staurolite, and ilmenite, indicating synkinematic garnet growth. Garnet is rich in almandine, with $Alm_{72\text{-}82}$, $Grs_{06\text{-}16}$, $Prp_{03\text{-}13}$ and $Sps_{01\text{-}07}$ (fig. 6*a*, *b*). The garnet zonation is of prograde origin with higher spessartine and grossular contents in cores than at rims, while almandine and pyrope contents increase toward the rim. The metapelites display several textural types of muscovite within and crosscutting the foliation, but all have similar chemical composition (Si = 3.08 to 3.12 pfu; X_{Fe} = 0.62 to 0.69). Biotite is only present in some of the studied metapelites and is strongly chloritized in most samples. Biotite (X_{Fe} = 0.58 to 0.62), which is only slightly affected by retrogression, shows exsolution of ilmenite at the rims and displays a low Ti content (0.11–0.12 pfu). Plagioclase is common as a matrix mineral in almost all samples except in sample Z 270-6, where plagioclase as well as kyanite only occur as tiny inclusions in garnet. The An content increases slightly from core to rim in the matrix plagioclase (An_{44}-An_{47}) and in plagioclase inclusions in garnet (An_{22}-An_{28}). In some rocks, kyanite and garnet contain inclusions of staurolite (X_{Fe} = 0.85 to 0.93; ZnO = 1.3 to 2.4 wt%; fig. 5*d*). Retrograde chloritoid (X_{Fe} = 0.91 to 0.92) occurs along cracks in garnet and replaces staurolite inclusions (fig. 5*e*). Additionally, chloritoid surrounds and replaces staurolite in the matrix. Retrograde chlorite (X_{Fe} = 0.56 to 0.77) partially replaces biotite and/or garnet in all metapelites.

Lufilian Arc: Whiteschists and Solwezi Dome Rocks. The whiteschists of the Lufilian Arc contain the mineral assemblages talc-kyanite-quartz-tourmaline-hematite-rutile. The greenish whiteschist variety of the Chowe River was not found, but a brownish variety with the retrograde assemblage phlogopite-phengite-quartz-kyanite-chlorite occurs. Kyanite is centimeter sized whereas all other minerals are in the millimeter range. Kyanite

Table 1. Mineral Assemblages of Analyzed Samples

Sample	Type	Location	Amp	Bt	Chl	Crd	Ctd	Grt	Ky	Ms	Pl	St	Tlc
8HC 234	+	Z		x	x				x		x		x
Z 103-2	−	Z	x	x	x	x			x			x	x
Z 103-12	+	Z			x	x			x				
Z 270-5	−	Z		x	x			x	x	x	x	x	
Z 270-6	−	Z			x		x	x	x	x	x	x	
Z 272-1b	+	Z			x				x	x	x		x
Z 220-1	−	L	x	x						x	x		
Z 220-7	+	L		x	x				x	x			
Z 221-1	−	L		x				x	x		x		
Z 222-1	−	L	x	x				x			x		
Z 223-1	−	L	x					x			x		
Z 230-1	+	L							x				x
Z 241-1	−	L	x	x							x		
Z 244-1	+	L							x				x
Z 245-1	+	L							x				x

Note. Plus sign = whiteschist; minus sign = nonwhiteschist; Z = Zambesi Belt sample; L = Lufilian Arc sample.

usually has inclusion-free cores and poikiloblastic rims that are clouded with inclusions. Talc has lower Al contents and X_{Fe} compared with the Chowe River samples (Al = 0.12 to 0.15, rarely up to ~0.20 pfu; X_{Fe} = 0.005 to 0.007). Tourmaline is Fe-rich dravite with greenish cores and yellow rims. Hematite is very common and can constitute up to 20% of the rock. Magnesian chlorite was not found in any of the investigated whiteschists sensu stricto. The phengite of the brownish variety has Si contents of about 3.25 pfu and contains 0.5 to 1.0 wt% Na_2O. The phlogopite (X_{Fe} = 0.05 to 0.06) contains ~0.8 wt% TiO_2 and ~0.5 wt% Na_2O. Within the brownish variety, no talc was found, and hematite is less common, but Mg chlorite occurs as a minor phase.

The biotite-kyanite-garnet gneiss contains the mineral assemblages biotite-quartz-plagioclase-kyanite-garnet. Kyanite occurs in sizes up to 1 cm, while all other minerals have grain sizes in the millimeter range. Greenish biotite grew within the foliation but may also crosscut it. Biotite has a greenish color and matrix biotite differs chemically from biotite associated with garnet. Matrix biotite (X_{Fe} ~0.36) has $TiO_2 > 1$ wt%, while biotite associated with garnet (X_{Fe} ~0.38) has $TiO_2 < 1$ wt%. Garnet is almandine rich, with Alm_{62-66}, Grs_{11-12}, Prp_{18-24}, and Sps_{1-5}. The garnet zonation is restricted to a small retrograde rim with slightly higher pyrope contents in the cores than at rims, while almandine and spessartine contents and X_{Fe} (from 0.72 to 0.78) increase toward the rim (fig. 6*c*). Plagioclase that occurs close to garnet is slightly zoned with An_{27} in the core and An_{30} at the rim. Matrix plagioclase (An_{24}) shows no zoning. Accessory phases include muscovite inclusions in quartz and plagioclase, apatite, and magnetite.

The mineral assemblages of the garnet amphibolites are amphibole-quartz-garnet-plagioclase ± biotite ± scapolite ± epidote. The amphibole is a ferropargasite (X_{Fe} ~0.55 to 0.60) with TiO_2 contents between 0.5 and 0.9 wt%. Most amphiboles contain relics of former pyroxenes in the cores; in some amphiboles tiny inclusions of titanite occur. Garnet is slightly zoned and shows preserved growth zoning and retrograde zoning near rims. Core-rim compositions are Alm_{56-57} to Alm_{57-60}, Grs_{26-28} to Grs_{22-30}, Prp_{09-11} to Prp_{11-12}, and Sps_{05-09} to Sps_{03-06}. The X_{Fe} value ranges from 0.80 to 0.88, with higher X_{Fe} in the core than at the retrograde rims. Plagioclase is zoned with An_{44} in the core and An_{50-56} near the rim. Where plagioclase is associated with garnet and biotite, the An content can increase up to An_{65}. In sample Z 223-1, only albitic plagioclase (An_{10}) is preserved as inclusion in amphibole. In this rock, scapolite occurs with ~1 wt% Cl, associated with epidote with TiO_2 ~0.9 wt%. Biotite (X_{Fe} = 0.44 to 0.45) has TiO_2 contents of 2.2 to 2.3 wt%. Biotite is usually associated with garnet and plagioclase (fig. 5*f*). Ilmenite, magnetite, titanite, and apatite are common accessories.

Reaction History and *PT* Evolution

Zambezi Belt: Chowe River Rocks. Mineral assemblages of the different rock types of the Chowe River section, including whiteschist, anthophyllite-kyanite-cordierite gneiss, and metapelite, indicate high metamorphic temperatures and pressures. These rock types also have common reaction textures pointing to decompression after peak metamorphism (e.g., cordierite rims surround kyanite). These shared characteristics as well as the close association of the rocks in the field indicate

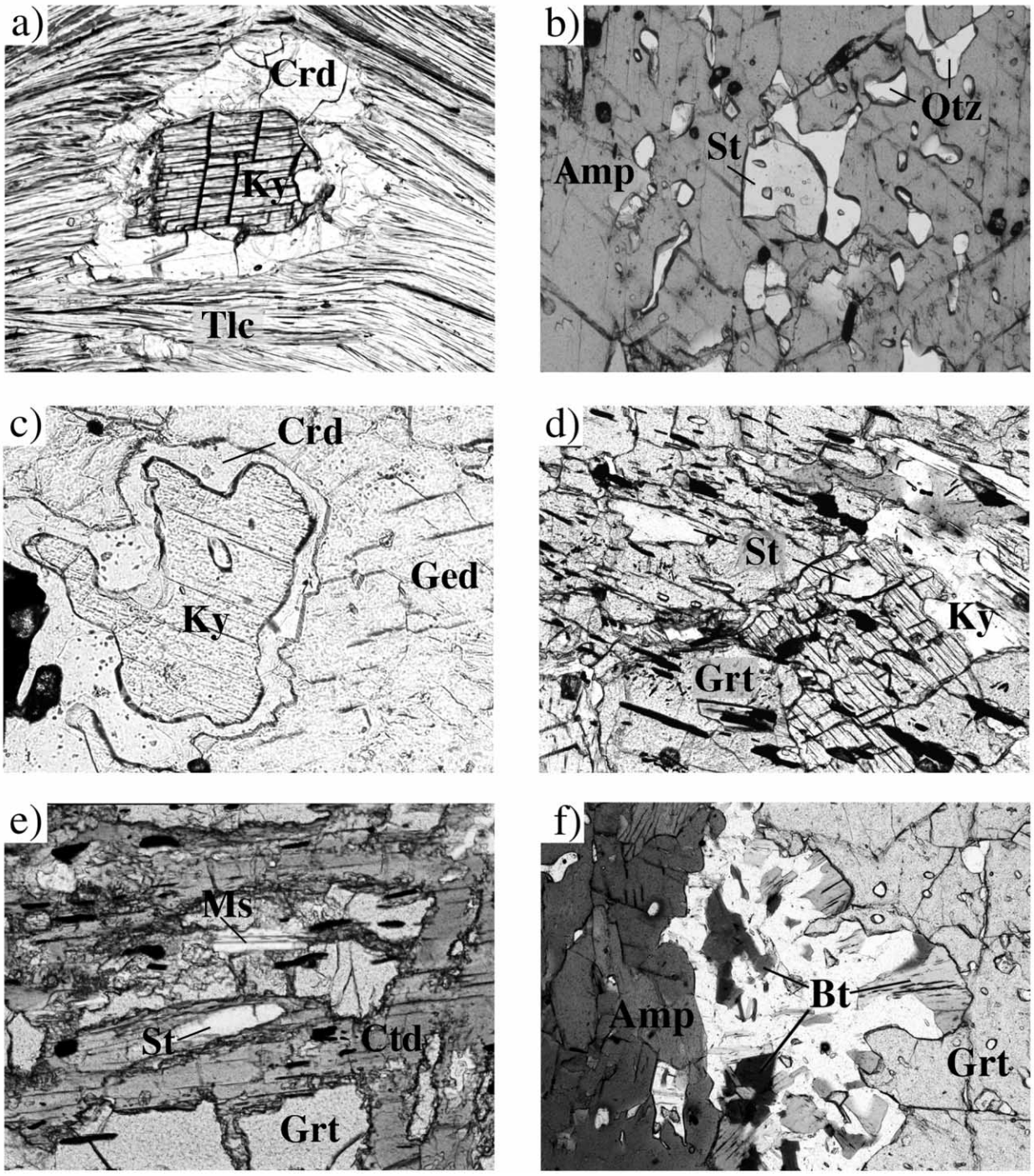

Figure 5. *a*, Kyanite in a matrix of talc and quartz surrounded by a cordierite rim. Quartz is not shown. Chowe River area, whiteschist (Z 103-12). Field of view ca. 1 mm. *b*, Staurolite relic as inclusion in hornblende. Chowe River area, Ged-Crd-Ky gneiss (Z 103-2). Field of view ca. 1 mm. *c*, Kyanite and anthophyllite are separated by a cordierite rim; black mineral is ilmenite. Chowe River area, Ged-Crd-Ky gneiss (Z 103-2). Field of view ca. 0.75 mm. *d*, Staurolite as inclusion in porphyroblastic garnet and kyanite. Black mineral is ilmenite, white lath is muscovite, and the dark gray mineral is chlorite. Chowe River area, metapelite (Z 270-5). Field of view ca. 1.5 mm. *e*, Late-stage chloritoid grown along cracks in garnet and surrounding former staurolite inclusions. Chowe River area, metapelite (Z 270-6). Field of view ca. 0.75 mm. *f*, Garnet resorption and biotite-plagioclase intergrowth. Biotite and plagioclase forming rims between garnet and amphibole. Solwezi Dome, Grt-amphibolite (Z 222-1). Field of view ca. 1 mm.

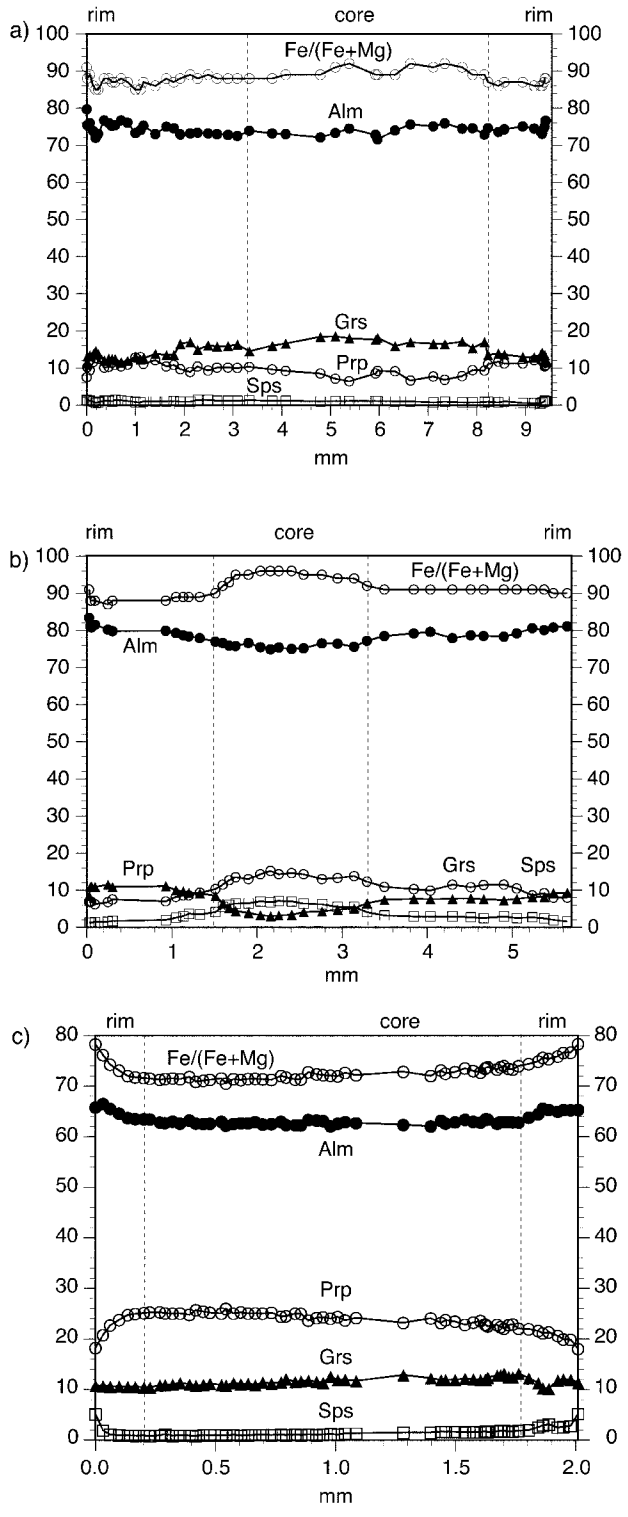

Figure 6. Garnet zoning profiles: *a*, metapelite with matrix Ky (Z 270-5); *b*, metapelite with Ky only as inclusion in Grt (Z 270-6) from the Chowe River section; and *c*, Bt-Ky-Grt gneiss from the Solwezi Dome (Z 221-1).

that they experienced the same metamorphic evolution. Most information on the different stages of the metamorphic evolution can be obtained from the metapelites, while some crucial reactions are also preserved in the whiteschists and anthophyllite-kyanite-cordierite gneisses.

Peak metamorphic conditions were estimated with the garnet-biotite Fe-Mg exchange thermometer (Kleemann and Reinhardt 1994) and the equilibrium garnet-alumosilicate-quartz-plagioclase (GASP; Koziol 1989).

Prograde Evolution. A prograde reaction texture is preserved in the anthophyllite-cordierite-kyanite gneiss, in which staurolite forms inclusions in amphiboles (fig. 5*b*). These relics are attributed to the reaction

$$\text{staurolite} + \text{chlorite} \rightarrow \text{anthophyllite} + \text{kyanite}. \quad (1)$$

Based on observations of natural assemblages in amphibolites in New Hampshire, Spear and Rumble (1986) proposed a petrogenetic grid (FMASH system) placing this reaction at about 550°–600°C (fig. 7).

The next preserved step on the *PT* path is a staurolite-consuming reaction in Fe-rich metapelites. Inclusions of staurolite in kyanite and garnet indicate the FASH reaction

$$\text{Fe-staurolite} + \text{quartz} \rightarrow \text{garnet} + \text{kyanite} \quad (2)$$

has been overstepped (fig. 5*d*). However, the terminal stability reaction for staurolite in the KFMASH system,

$$\text{staurolite} + \text{muscovite} + \text{quartz} \rightarrow \text{garnet} + \text{kyanite} + \text{biotite}, \quad (3)$$

(Spear and Cheney 1989) was not reached, since staurolite relics are preserved in the muscovite + quartz matrix. This limits the metamorphic temperatures to below ca. 710°C (fig. 7).

Peak-Metamorphic Conditions. Two different samples of metapelites were investigated that have slightly different mineral assemblages. One sample contains kyanite in the matrix; in the other kyanite occurs only as inclusions in garnet. The outer parts of garnet in the latter type (sample Z 270-6) contain inclusions of quartz, kyanite, and plagioclase, a mineral assemblage suitable for GASP barometry. Pressure estimates for the later stages of garnet growth are based on these inclusions. However, the estimates suffer from the lack of well-constrained

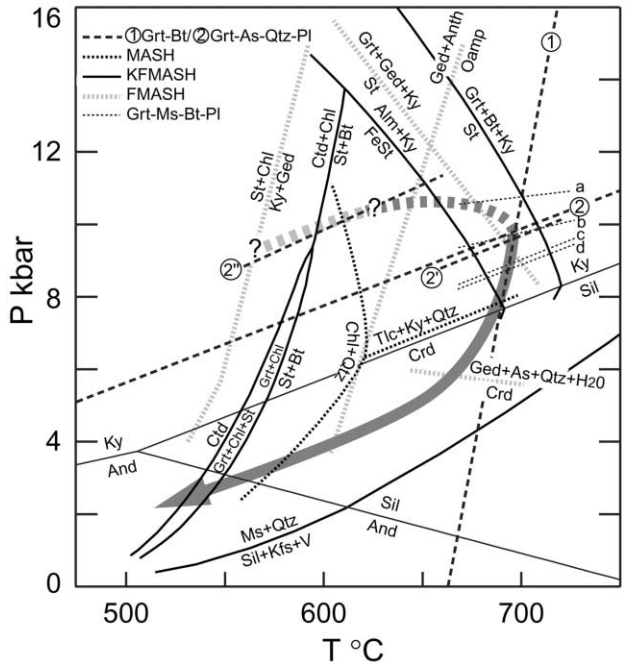

Figure 7. *PT* diagram with relevant reaction curves for the *PT* evolution of the Chowe River section. Al_2SiO_5 triple point after Holdaway (1971), MASH system for whiteschists after Massonne (1989), KFMASH system for metapelites after Spear and Cheney (1989), and FMASH system for cordierite-anthophyllite gneisses modified after Spear and Rumble (1986). *1*, Garnet-biotite thermometry (Kleemann and Reinhardt 1994); *2*, garnet-alumosilicate-quartz-plagioclase equilibrium (Koziol 1989) using matrix plagioclase and matrix garnet rim (Z 270-5); *2′*, using rim of plagioclase inclusion and surrounding garnet rim (Z 270-6); *2″*, using core of plagioclase inclusion in garnet (Z 270-6) as explained in text. *a–d*, Garnet-muscovite-biotite-plagioclase barometry (*a*, Powell and Holland 1988; *b*, Mg, Hoisch 1990; *c*, Hodges and Crowley 1985; *d*, Fe, Hoisch 1990).

temperature information for this stage of the *PT* evolution. Because the inclusions occur only in the outer parts of garnet, it is assumed that they were probably trapped at or above 600°C and not close to the Grt-in temperature. According to the preserved prograde garnet growth zoning, which shows a slightly higher Grs content and X_{Fe} value in the core than in the rim (fig. 6*b*), the prograde heating path seems to have had a flatter dP/dT slope than the GASP-equilibrium curve (fig. 7). Plagioclase inclusions (ca. 0.10–0.01 mm) are zoned from core (An_{21}) toward the rim (An_{32}), while the surrounding garnet is zoned toward the inclusion (Grs_{14} and Grs_{11}). Assuming that the rims of the plagioclase inclusions (An_{32}) were in equilibrium with the surrounding Grt rims (Grs_{11}) and that the Pl cores (An_{21}) were in equilibrium with those parts of the garnet not affected by the late stage equilibration with the inclusions (Grs_{14}), both composition pairs were used for pressure estimates. The pressure estimates of 10–11 kbar using core compositions of Pl inclusion and corresponding garnet compositions and an assumed temperature of about 600°–650°C are attributed to a stage of the prograde *PT* evolution (curve 2″ in fig. 7). The combination of the inclusion rim with the surrounding garnet rim results in GASP equilibrium curve ca. 2 kbar lower than the one of the core estimates (curve 2′ in fig. 7). The latter pressure estimate is similar to that for peak metamorphism, which was calculated from rim compositions of minerals (Grt, Pl, Bt) of rock samples that contain kyanite in the matrix (sample Z 270-5). These peak estimates reveal conditions of about 700° ± 25°C at around 10 ± 1 kbar (curves 1 and 2 in fig. 7). Garnet-muscovite-biotite-plagioclase barometry (Hodges and Crowley 1985; Powell and Holland 1988; Hoisch 1990) yields similar estimates of ca. 9 to 11 ± 1 kbar at 700° ± 25°C (curves a–d in fig. 7). The high Al_2O_3 content of talc in the whiteschists is in agreement with the high temperatures obtained (Massonne 1995).

Retrograde Evolution. Three different stages of the retrograde *PT* path can be deduced from mineral reaction textures. The first stage is based on a reaction texture in whiteschist, where cordierite forms rims surrounding kyanite in a talc-quartz matrix (fig. 5*a*), which can be attributed to the decompression reaction

$$\text{talc} + \text{kyanite} + \text{quartz} \rightarrow \text{cordierite} \qquad (4)$$

(Schreyer and Seifert 1969; Massonne 1989). Also in the anthophyllite-cordierite-kyanite gneiss, cordierite forms rims surrounding kyanite (fig. 5*c*). Applying the FMASH grids of Spear and Rumble (1986) and Schumacher and Robinson (1987), this cordierite rim is interpreted as a decompression texture as well (fig. 7). The corresponding reaction is

$$\text{anthophyllite} + \text{kyanite} + \text{quartz} \rightarrow \text{cordierite}. \qquad (5)$$

A third retrograde stage was found in metapelites, where chloritoid replaces staurolite and garnet (fig.

5*e*). First, chlorite was produced by the resorption of biotite according to the reaction

$$\text{staurolite} + \text{biotite} + \text{quartz} + H_2O \rightarrow \text{chlorite} + \text{garnet} + \text{muscovite}. \quad (6)$$

Subsequently, chloritoid is formed by the reaction

$$\text{garnet} + \text{staurolite} + \text{chlorite} \rightarrow \text{chloritoid} + \text{muscovite} + \text{quartz}. \quad (7)$$

The grid of Spear and Cheney (1989) places these reactions between 550° and 600°C (fig. 7).

PT *Path*. The combination of the petrological features described above allows the reconstruction of a clockwise *PT* path with peak metamorphic conditions near 10 ± 1 kbar and temperatures of ca. 700° ± 25°C (fig. 7). The proposed slope of the *PT* path with constant or slightly decreasing pressures during prograde heating is supported by the preserved Grs-growth zoning in metapelitic garnet.

Lufilian Arc: Solwezi Dome Rocks. Outcrops with fresh rocks are rare because of the strong weathering and the widespread lateritic cover, and thus, the amount of samples and lithologies that can be used for petrological investigations are limited. However, peak metamorphic conditions are estimated using the same geothermobarometers as described above as well as the garnet-hornblende Fe-Mg exchange thermometer (Graham and Powell 1984) and the garnet-quartz-plagioclase-biotite equilibrium (Hoisch 1990).

Metamorphic Evolution and PT *Path*. The chemical profiles of garnets of the investigated amphibolites and gneisses show flat patterns as well as minor growth zoning, but usually only the outer part of the garnet rims are affected by retrogression. Using the most Mg-rich part from the prograde garnet zoning with matrix amphiboles (amphibolite) and cores of homogenized garnets with matrix plagioclase cores (biotite-kyanite-garnet gneiss), estimates of peak-conditions give ca. 740° to 755° ± 25°C at about 13 ± 1 kbar (fig. 8).

Information about the metamorphic evolution is only given through the resorption of garnet. In amphibolites, garnet resorption is probably related to the reaction

$$\text{garnet} + \text{amphibole} \rightarrow \text{biotite} + \text{plagioclase} + \text{quartz}, \quad (8)$$

which resulted in plagioclase-biotite ± quartz coronas between garnet and amphibole (fig. 5*f*). Since

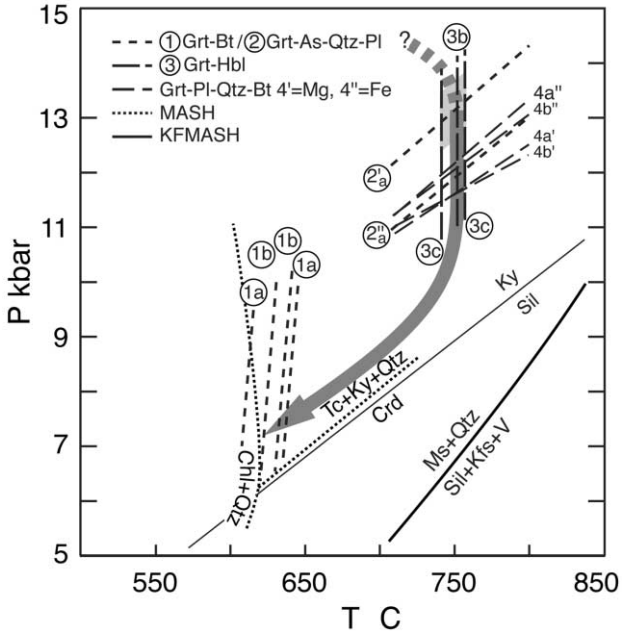

Figure 8. *PT* diagram with relevant reaction curves for the Solwezi Dome rocks and Lufilian Arc whiteschists. KFMASH system after Spear and Cheney (1989), MASH system for whiteschists after Massonne (1989). Thermobarometric results: *a* = Z 221-1; *b* = Z 222-1; *c* = 223-1 curve; *1*, garnet-biotite thermometry (Kleemann and Reinhardt 1994); *2*, garnet-alumosilicate-quartz-plagioclase equilibrium (Koziol 1989) with 2′ indicating peak and 2″ retrograde conditions; *3*, garnet-hornblende thermometry (Graham and Powell 1984); *4*, garnet-plagioclase-quartz-biotite equilibrium (Hoisch 1990). Thick arrows show possible *PT* paths. Shaded areas indicate uncertainties of *PT* estimates.

only little biotite was formed, the necessary K content for the biotite formation could have come from the related amphibole consumption (>1 wt% K_2O). Within the biotite-kyanite-garnet gneiss, garnet resorption can be attributed to the reaction

$$\text{grossular} + \text{quartz} + \text{kyanite} \rightarrow \text{anorthite} \quad (9)$$

and indicates decompression (like reaction [8]). The newly formed plagioclase displays higher An contents (An_{30}) than the peak stage plagioclase (An_{24}). Estimates obtained from products of reactions (8) and (9) as well as matrix biotite (biotite-kyanite-garnet gneiss) and the rim compositions of garnet point to lower temperatures of ca. 610° to 650° ± 25°C and a pressures drop of at least 2 kbar (fig. 8).

Combining the *PT* estimates and decompression features obtained from the amphibolites and gneisses indicates a clockwise *PT* evolution with

peak metamorphic conditions of about 13 ± 1 kbar and temperatures of ca. 750° ± 25°C (fig. 8). *PT* conditions of cooling are about 630° ± 25°C at pressures below 9–10 kbar. Further cooling and exhumation is not documented in mineral textures and chemistry.

Discussion and Comparison with Previous Studies. Peak metamorphic conditions were 700° ± 25°C at 10 ± 1 kbar in the Chowe River section in the Zambezi Belt and 750° ± 25°C at 13 ± 1 kbar for some whiteschist occurrences of the Lufilian Arc. A clockwise *PT* path characterizes both areas. Subsequent to the thermal peak, the rocks experienced nearly isothermal decompression. Both decompression paths are interpreted to be the consequence of a significant, early tectonic crustal thickening event, which was followed by rapid erosion and/or tectonic uplift.

The petrological results of the present study are supported by previous studies of different parts of the Zambezi Belt and Lufilian Arc. Regarding the Zambezi Belt, Johnson and Oliver (1998) estimated minimum *PT* conditions of about 590°C and 13 kbar for a yoderite-bearing whiteschist terrane in the Chewore Inliers (fig. 2). In addition, the authors calculated metamorphic peak conditions of 700°C and 10.5 kbar for Grt-bearing amphibolites and metapelites in a neighboring ophiolite terrane. Similar estimates (600°–750°C/8–9 kbar) are given by Goscombe et al. (1998) for their M2 event in several terranes of the Chewore Inliers. The M2 event was followed by an almost isothermal decompression that is similar to the metamorphic evolution of the Chowe River section reported here. Since Vrána and Barr (1972) did not find the cordierite reaction rims in whiteschists, they proposed a more synchronous exhumation and cooling of the Chowe River whiteschists than the data of the present study imply. Cosi et al. (1992) reported for the Lufilian Arc a *PT* evolution defined by two metamorphic stages using phase-petrological observations obtained from amphibolites, whiteschists, and metapelites sampled over the entire Domes Region. They estimated a high-pressure amphibolite facies stage with temperatures between 600° and 700°C at pressures below 13 kbar and late-stage, low-pressure amphibolite facies overprint with temperatures of 600°–700°C and pressures between 5 and 6 kbar.

Cosi et al. (1992) mentioned whiteschists containing garnet and eclogites containing omphacite (X_{Jd}35 – 40 mol %) occurring in the Domes Region. In contrast to that, the whiteschist metamorphism from the outcrops studied here does not show evidences for an eclogite facies stage. On the contrary, the occurrence of albite in the whiteschist assemblage (Zambezi Belt) precludes very high pressures. All whiteschists formed at high-grade amphibolite facies conditions; however, there are differences between the mineral assemblages and mineral textures found in whiteschists of the Zambezi Belt and of the Lufilian Arc. The Zambezi Belt samples display textures formed by reactions at two different metamorphic stages after peak metamorphism: cordierite formation during decompression and the Mg-chlorite formation during subsequent cooling. These stages are also documented within the associated rocks, again with cordierite formation during decompression, and with chloritoid formation during cooling (fig. 7). The investigated rocks of the Lufilian Arc only contain information about peak metamorphism and one stage of the retrograde evolution, which was found in nonwhiteschists only. The pressure drop during the documented retrograde evolution was not strong enough to form cordierite in whiteschists, and the temperature conditions at which the rocks partially re-equilibrated during exhumation were above the Mg chlorite + quartz stability field for the MASH system (fig. 8).

Geochronology

The U-Pb systematics of metamorphic monazite are used to date the peak stage of metamorphism, while zircons are used to date the formation of the basement of the Lufilian Arc domes. Rb-Sr cooling ages were determined to evaluate whether the basement was affected by the same metamorphism as the overlying Katangan rocks and to reconstruct the cooling history of the area. Monazite-forming reactions described for metapelitic rocks are starting at lower amphibolite facies conditions (e.g., Smith and Barreiro 1990; Bingen et al. 1996). Compared with zircon, monazite is less prone to Pb-loss at high-grade metamorphic conditions. The closure temperature of the U-Th-Pb system in monazite was estimated at about 700° to 750°C (Mezger 1990; Parrish 1990), but it was also argued that it is higher than 800°C (Schenk 1980; Spear and Parrish 1996). Thus, monazite that grew during metamorphism is ideal to date the peak stage of amphibolite facies metamorphism (for details of sample preparation and isotope analysis, see app. B in the online edition of *The Journal of Geology*)

Sample Description. One whiteschist sample of the greenish variety (Z 271-2) of the chlorite schists unit of the Rufunsa Metavolcanic Formation was selected to constrain the time of metamorphism within the central Zambezi Belt. To determine the age of metamorphism in the Lufilian Arc, two whiteschists of the grayish variety, from the Ka-

Table 2. U-Pb Analytical Results for Monazite and Zircon from Zamberi Belt and Lufilian Arc

Sample	Mineral	Size (μm)	Rock type	Weight (mg)	Composition U (ppm)	Composition Pb (ppm)	Isotopic ratios[a] $^{206}Pb/^{204}Pb$	$^{206}Pb/^{208}Pb$	$^{207}Pb/^{206}Pb$	$^{206}Pb/^{238}U$	$^{207}Pb/^{235}U$	Correlation coefficient	Apparent ages (Ma) $^{206}Pb/^{238}U$	$^{207}Pb/^{235}U$	$^{207}Pb/^{206}Pb$
Zambesi Belt:															
Z 271-2	Mnz	250–350	Whiteschist	.50	221	298	3502	.06219	.05484 (.28)	.09078 (.47)	.6864 (.55)	.85	560.2	530.6	405.6
Z 271-2	Mnz	Mixed	Whiteschist	1.63	292	302	1907	.0816	.05599 (.29)	.08893 (.21)	.6866 (.37)	.64	549.2	530.8	425.1
Z 271-2	Mnz	60–75	Whiteschist	.16	575	304	3623	.1750	.05403 (.06)	.09011 (.18)	.6713 (.19)	.88	556.2	521.5	372.3
Lufilian Arc:															
Z 220-1	Zrn_Z1	75–100	Basement gneis	.10	571	185	4769	13.70	.1130 (.05)	.3154 (.19)	4.914 (.19)	.93	1767	1805	1848
Z 220-1	Zrn_Z2	75–100	Basement gneis	.15	467	148	3642	14.59	.1125 (.05)	.3090 (.18)	4.795 (.19)	.92	1736	1784	1841
Z 220-1	Zrn_Z3	75–100	Basement gneis	.14	429	136	3361	12.16	.1129 (.05)	.3057 (.18)	4.761 (.19)	.91	1720	1778	1847
Z 220-1	Zrn_Z4	<60	Basement gneis	.08	441	141	1256	13.61	.1118 (.07)	.3012 (.18)	4.643 (.20)	.86	1697	1757	1829
Z 220-1	Zrn_Z5	150–250	Basement gneis	.80	638	195	1887	11.46	.1116 (.06)	.2883 (.40)	4.436 (.40)	.99	1633	1719	1826
Z 220-9	Mnz	150–200	Whiteschist	.79	222	590	4129	.02925	.05314 (.11)	.08707 (.18)	.6379 (.22)	.71	538.2	501.0	334.6
Z 221-7	Mnz	100–150	Bt-ky-grt gneis	.18	2810	363	8055	1.466	.05797 (.06)	.08566 (.20)	.6847 (.20)	.93	529.8	529.6	528.7
Z 230-1	Mnz	400–500	Whiteschist	.49	34.2	51.0	384.7	.05376	.05734 (.33)	.08706 (.19)	.6883 (.42)	.61	538.1	531.8	504.8
Z 230-1	Mnz	75–100	Whiteschist	.15	38.0	77.6	309.7	.03879	.05587 (.48)	.08777 (.26)	.6761 (.64)	.77	542.3	524.4	447.2
Z 241-1	Zrn_Za	60–75	Basement gneis	.07	74.3	27.7	429.3	4.700	.1139 (.14)	.3179 (.27)	4.992 (.33)	.90	1779	1818	1862
Z 241-1	Zrn_Zb	<60	Basement gneis	.07	332	120	2670	4.537	.1141 (.05)	.3141 (.15)	4.941 (.16)	.76	1759	1808	1866
Z 241-1	Zrn_Zc	150–250	Basement gneis	.30	142	53.9	1410	4.615	.1141 (.07)	.3218 (.19)	5.064 (.21)	.90	1798	1830	1866
Z 244-1	Mnz	75–100	Whiteschist	.04	255	596	752.5	.03366	.05608 (.27)	.08754 (.20)	.6768 (.37)	.62	540.9	524.9	455.4

[a] $^{206}Pb/^{204}Pb$ is the measured ratio, all others are calculated, correction for blank, common Pb and fractionation. Number in parentheses is the relative 2σ uncertainty in %.

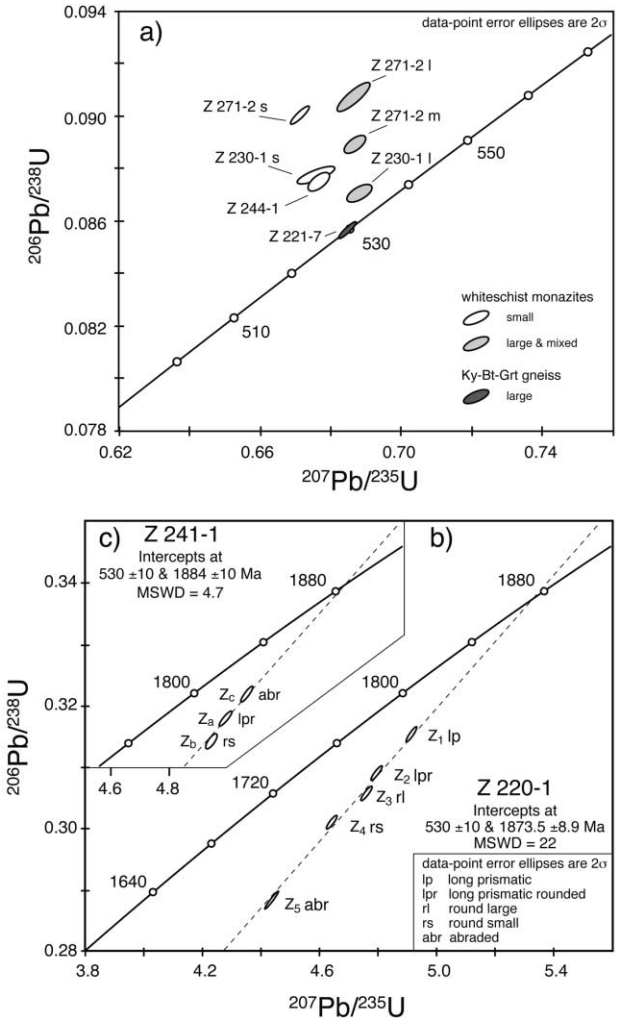

Figure 9. Concordia diagrams for (*a*) monazite analyses of whiteschists (small size fractions = *white*; large size fractions = *gray*) and garnet-biotite-kyanite gneiss (*dark gray*), (*b*) zircon analyses of the Solwezi Dome basement gneiss (Z 220-1), and (*c*) zircon analyses of the Solwezi Dome basement gneiss (Z 220-1). Sample numbers are indicated.

bompo (Z 244-1) and the Mwombezhi Dome (Z 230-1), and one whiteschist of the brownish variety (Z 220-9) as well as one biotite-kyanite-garnet gneiss (Z221-7) from the Solwezi Dome were collected. All samples belong to the lower units of the Roan Group. The basement rocks were sampled at the Kabompo Dome (plagioclase-quartz-biotite-hornblende-epidote gneiss; Z 241-1) and at the Solwezi Dome (plagioclase-quartz-biotite-muscovite-epidote-tourmaline gneiss; Z 220-1).

Results of U-Pb and Rb-Sr Geochronology. *Monazite Ages.* Monazite typically has high Th/U ratios with more than 5 wt% ThO_2 and much less than 1 wt% UO_2 (Köppel 1974). Monazites that grew under highly oxidizing conditions should incorporate even more Th than U and thus also ^{230}Th (a short-lived intermediate daughter of ^{238}U), since U occurs under such conditions mainly as U^{6+} and is therefore not suitable for incorporation into the monazite structure. The decay from ^{230}Th to ^{206}Pb (half-life ca. 75,000 yr) produces $^{206}Pb/^{238}U$ ages that are too old because thorogenic ^{206}Pb is added to the uranogenic ^{206}Pb (Schärer 1984). Therefore, the $^{207}Pb/^{235}U$ age represents the best estimate for the age of monazites, specially if they have high Th/U ratios due to oxidizing conditions (Parrish 1990; Tomascak et al. 1996). Whiteschists have highly oxidized mineral assemblages with almost all Fe bound in hematite resulting in the typical high-Mg silicate assemblages. Multivalent ions mainly occur in their highest oxidation state (e.g., Johnson and Oliver 2002). Thus, the high Th/U ratios (50–120) of monazites from the whiteschists (table B11) suggest that excess ^{206}Pb may cause reverse discordance. A correction for excess ^{206}Pb is not possible for metamorphic monazites because it is not possible to evaluate which minerals were in equilibrium with monazite during its formation (Parrish 1990), and thus, it is not possible to estimate how much of the excess ^{206}Pb in the whole rock was available for incorporation into monazite during its growth. In order to evaluate the significance of the $^{207}Pb/^{235}U$ ages of whiteschist monazites, different grain size fractions as well as monazites from the biotite-kyanite-garnet gneiss (Z 221-7) were analyzed (table 2).

From all samples only clear and subhedral to round monazite crystals were selected for U-Pb geochronology. All monazite fractions of the investigated whiteschists yield strongly reverse discordant ages (fig. 9*a*). The fractions of the Chowe River sample (Z271-2) with the larger grain sizes (mixed and 250–350 μm) yield identical $^{207}Pb/^{235}U$ ages with 531 ± 2 Ma and 531 ± 3 Ma but vary strongly in the $^{206}Pb/^{238}U$ ratios (table 2). The smaller size fraction (60–75 μm) has a younger $^{207}Pb/^{235}U$ age with 522 ± 2 Ma and a similar $^{206}Pb/^{238}U$ age. The different size fractions of sample Z 230-1 (Lufilian Arc) yield the same $^{207}Pb/^{235}U$ age range with 532 ± 2 Ma (400–500 μm) and 524 ± 3 Ma (75–100 μm) as well as variations in the $^{206}Pb/^{238}U$ ratios (table 2) compared with the monazites of Zambezi Belt (Z 271-2). The monazite fraction (75–100 μm) of sample Z 244-1 has a $^{207}Pb/^{235}U$ age of 525 ± 2 Ma, which is similar to the result of the other smaller size fractions. The monazites of sample Z 220-9 (150–200 μm) yield a $^{207}Pb/^{235}U$ age of 501 ± 2 Ma, which is much younger than all other results (table

Table 3. Rb-Sr Isotope Analyses for Lufilian Arc Samples

Sample and type	Rb (ppm)	Sr (ppm)	$^{87}Rb/^{86}Sr$[a]	$^{87}Sr/^{86}Sr$[a]	Initial $^{87}Sr/^{86}Sr$	Age (Ma)[b]
Z 220-1:						
Muscovite	301	20.4	44.0	1.0287	.722	489.6 ± 4.8
Biotite	556	2.44	1134	8.4182	.722	476.3 ± 4.7
Plagioclase	104	622	.486	.72513		
Z 221-7:						
Biotite	323	3.59	309	2.7921	.726	468.8 ± 4.6
Plagioclase	.871	120	.0211	.72635		
Z 241-1:						
Biotite	1011	4.34	1190	8.7029	.739	469.7 ± 4.6
Plagioclase	175	565	.900	.74498		

[a] Ratios corrected for fractionation, spike, and blank as described in text. Uncertainties of isotopic ratios as described in text (not shown).
[b] Uncertainty in ages in million years at the 2σ confidence interval.

2). In contrast, the monazite fraction (100–150 μm) from the biotite-kyanite-garnet gneiss (Z 221-7) of the Solwezi Dome yields a concordant age of 529 ± 2 Ma (fig. 9*a*).

All $^{207}Pb/^{235}U$ ages of larger size fractions of monazites from whiteschsists range between 531 and 532 Ma. The analyses differ only in the $^{206}Pb/^{238}U$ ages (fig. 9*a*), indicating that thorogenic ^{206}Pb caused the strong and variable reverse discordance (e.g., Tomascak et al. 1996). The concordant age of sample Z 221-7 with 529 ± 2 Ma confirms the interpretation that the $^{207}Pb/^{235}U$ ages reflect the true ages, and since all other ages are identical within error, 529 ± 2 Ma is taken as the best age estimate for the peak of metamorphism. The smaller size fractions have younger $^{207}Pb/^{235}U$ ages, between 522 and 525 Ma (mean = 523 ± 2 Ma), with similar variations in the $^{206}Pb/^{238}U$ ages to those of the larger size fractions. The time between 530 and 523 displays the time span of monazite crystallization rather than cooling ages because metamorphic temperatures never reached values above the suggested closure temperatures of monazite. The monazite sample Z 220-9 with 501 ± 2 Ma is clearly younger than all other monazites; however, this rock displays the most intensive retrogression, and therefore this age is interpreted to be a result of late-stage fluid activity.

Cooling Ages. The results of the Rb-Sr dating of muscovite and biotite are given in table 3. The closure temperature for Rb-Sr has been estimated for muscovite at ca. 500° ± 50°C and for biotite at ca. 350°C (Hanson and Gast 1967; Dodson 1979).

For the biotite-kyanite-garnet gneiss (Z 221-7) sampled at the Solwezi Dome, the biotite-plagioclase isochron gives an age of 469 ± 5 Ma. The basement rock of the Solwezi Dome (Z 220-1) yields Rb-Sr ages of 490 ± 5 Ma for muscovite-plagioclase and 476 ± 5 Ma for biotite-plagioclase, indicating that both samples of the Solwezi Dome experienced the same cooling history since 500°C, and thus, both rocks were affected by the same tectonothermal event at about 530 Ma, dated with the U-Pb monazite ages. A biotite-plagioclase pair from the basement rock of the Kabompo Dome (Z 241-1) gives a Rb-Sr age of 470 ± 5 Ma, similar to the other biotite-plagioclase ages of this study, again indicating that the rocks experienced the same metamorphic event. Using ca. 530 Ma as the age of peak metamorphism with a peak temperature of ca. 750°C (Lufilian Arc) as well as the cooling ages for 500°C of ca. 490 Ma and for 350°C of ca. 470 Ma, the Lufilian Arc orogen cooled at a rate of ca. 6°–7°C/Ma.

Zircon Ages. U-Pb ages of zircons date the magmatic emplacement of the basement rocks of the Lufilian Arc domes. From the basement sample of the Solwezi Dome (Z 220-1), five fractions with different shapes and sizes were analyzed (table 2). Only pristine zircons were used, divided in groups with long prismatic (Z_1), long prismatic rounded (Z_2), spheric multiple-faceted (Z_3), very small crystals of spheric multiple-faceted (Z_4), and large, long prismatic crystals that were air abraded (Z_5). Air abrasion was used to obtain more concordant analyses by removing metamict parts or younger overgrowths (Krogh 1982; Mezger and Krogstad 1997). A discordia line through all five fractions has upper and lower intercept ages of 1863 ± 25 Ma and 414 ± 270 Ma with the close spacing of the analyses generating large uncertainties on both ages. The age of peak metamorphism with ca. 530 Ma, obtained from monazites of the overlying Katangan rocks, is within the error of the lower intercept age. Since the cover and the basement rocks experienced the same tectonothermal event, as indicated by the Rb-Sr mica ages, pinning of the discordia line through a 530 ± 10 Ma lower intercept seems to be reasonable and results in an upper intercept age of 1874 ± 9 Ma (fig. 9*b*). The air-abraded zircon

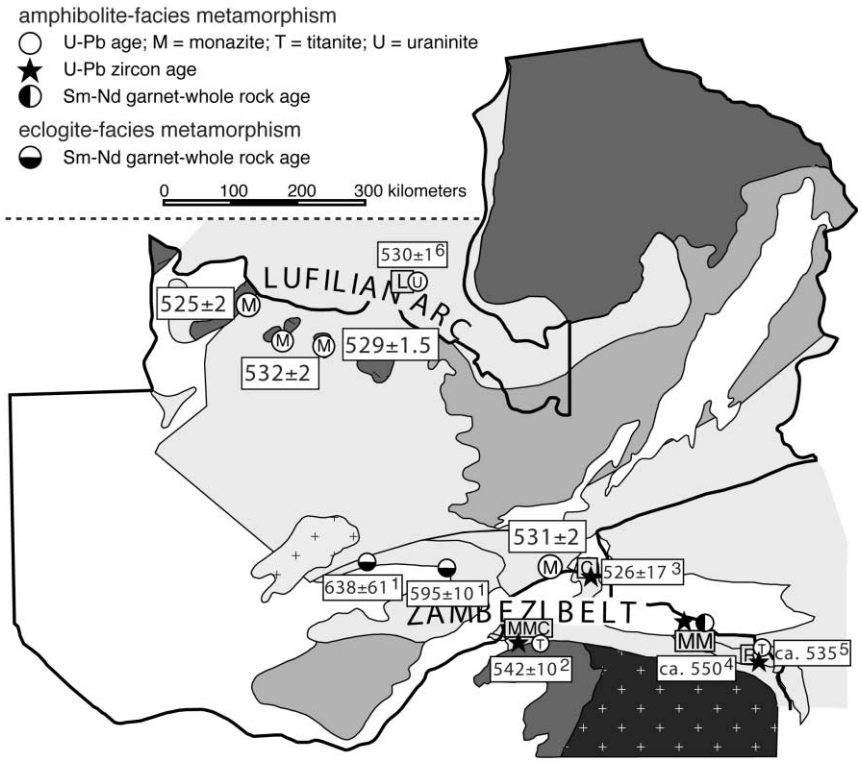

Figure 10. Geological map of Zambia, Northern Zimbabwe, and Western Moçambique showing the spatial distribution of determined ages of crustal thickening (amphibolite to eclogite facies) in the Lufilian Arc-Zambezi Belt orogen. Enlarged bold sample labels indicate the results of this study: *1* = John et al. 2003; *2* = Hanson et al. 1998; *3* = Goscombe et al. 2000; *4* = Müller 2002; *5* = Vinyu et al. 1999; *6* = Loris et al. 1997.

fraction gives the most discordant analysis (fig. 9*b*), which can be due to recrystallization of metamict zircons during amphibolite facies metamorphism (Mezger and Krogstad 1997). Three zircon fractions of sample Z 241-1 were used to define the time of crystallization of the Kabompo Dome basement. Only pristine zircons were used. The analyzed fractions (table 2) consist of long prismatic rounded (Z_a), spheric multiple-faceted (Z_b), and large long prismatic air-abraded crystals (Z_c). Since the Rb-Sr biotite age of this rock is identical with that of the Solwezi Dome rocks, the same assumption about the metamorphic evolution as for Z 220-1 were made. The three analyses define an upper intercept age of 1884 ± 10 Ma if the lower intercept is anchored at 530 ± 10 Ma (fig. 9*c*). Using only the three analyses, the upper intercept age is 1869 ± 120 Ma. The upper intercept ages of 1874 ± 9 Ma (Z 220-1, Solwezi Dome) and 1884 ± 10 Ma (Z 241-1, Kabompo Dome) are the best estimate for the basement formation of the Lufilian Arc domes. No evidence for another tectonothermal event between emplacement and peak metamorphism at ca. 530 Ma were found.

Comparison with Previous Studies and Discussion. The formation ages of the basement rocks within the Domes Region of 1874 ± 9 and 1884 ± 10 Ma is in agreement with the Palaeoproterozoic ages of basement rocks of the eastern Lufilian Arc, ranging from 2.0 to 1.8 Ga obtained by Rb-Sr whole rock and U-Pb SHRIMP dating (Cahen et al. 1984; Rainaud et al. 1999). However, with 1884 ± 10 Ma, the formation of the Kabompo Dome basement occurred ca. 50–60 m.yr. later than deduced from SHRIMP dating results of Key et al. (2001). The occurrence of ca. 1.2-Ga-old basement in the Domes Region, as suggested by Cosi et al. (1992), based mainly on a poorly constrained regional Rb-Sr isochron, is questionable in the light of the results of the present study. In addition, no evidence for a Mesoproterozoic metamorphic event was found that might have affected the rocks of the Domes Region.

A tectonothermal event between ca. 550 and 525

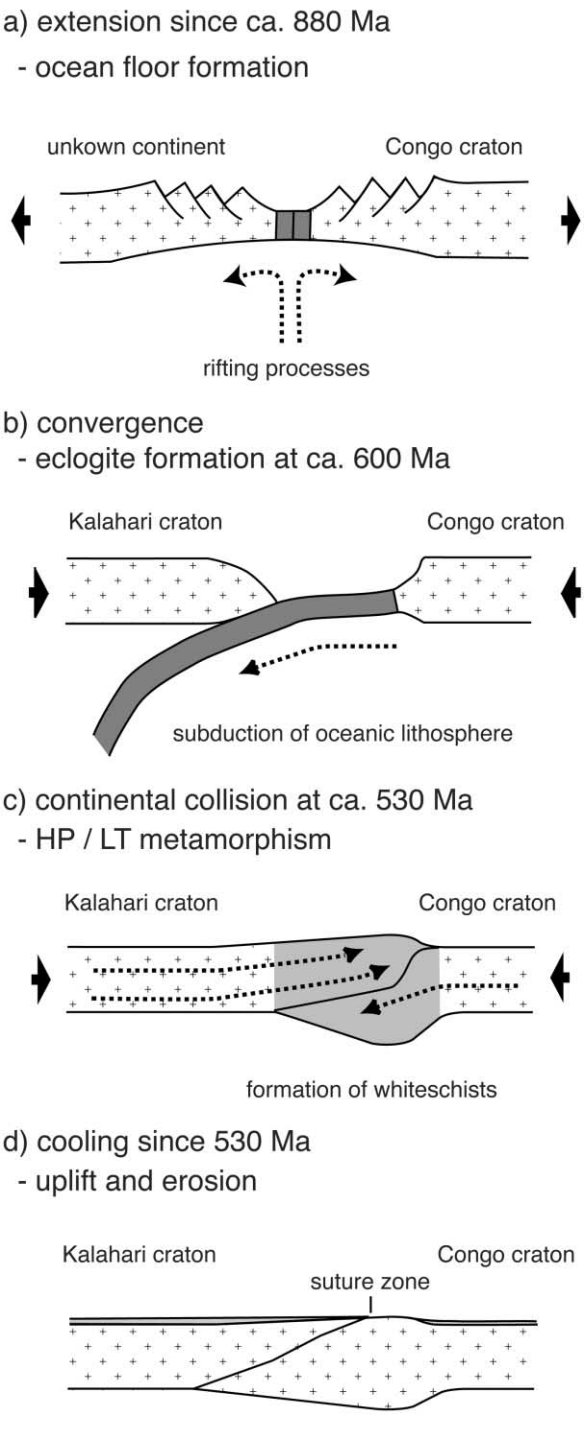

Figure 11. Illustration of the proposed evolution of the Pan-African Lufilian Arc–Zambezi Belt orogen: *a*, the extensional stadium is related to the dispersal of Rodinia and led to the formation of an ocean basin; *b*, during convergence between the Kalahari and Congo craton, the ocean basin closed; *c*, in the final stage of convergence, the Kalahari and Congo cratons collide, resulting in a continent-continent collision; *d*, the stage of cooling is dominated by denudation and uplift.

Ma has been dated at several localities of the entire Lufilian Arc–Zambezi Belt (fig. 10). Amphibolite to high-pressure granulite facies metamorphic events in the Zambezi Belt have been dated in the Rushinga Area around ca. 535 Ma (U-Pb zircon and titanite ages; Vinyu et al. 1999), in the Mavuradonha Mountains at ca. 550 Ma with 551 ± 7 to 545 ± 9 Ma (Pb-Pb zircon evaporation and Grt-wr Sm-Nd ages; Müller 2002), in the Chewore Inliers at 526 ± 17 Ma (SHRIMP analyses of zircon; Goscombe et al. 2000), and in the Makuti Metamorphic Complex around 542 ± 10 Ma (U-Pb zircon and titanite ages; Hanson et al. 1998). In addition, recrystallization of uraninite due to a tectonic event at around 530 ± 1 Ma has been dated with the U-Pb system at Lwiswishi, Lufilian Arc (Loris et al. 1997). All these ages are in a good agreement with the results of this study and thus point to one major crustal thickening event at ca. 530 Ma that affected the entire Lufilian Arc–Zambezi Belt orogen almost simultaneously (fig. 10). This interpretation is consistent with recent models of the Pan-African belts of central southern Africa. In these models an orogenic belt formed by continental collision between 560 and 540 Ma stretches from the Moçambique Belt either to the Damara Belt (e.g., Goscombe et al. 2000) or to the West Congo Belt (e.g., Porada and Berhorst 2000; fig. 1). Goscombe et al. (2000) concluded that the tectonic setting of this Pan-African orogenic belt is still unresolved. In contrast, Porada and Berhorst (2000) interpreted the Lufilian Arc and northern Zambezi Belt as originating together as a segment of a passive continental margin that belongs to the southern edge of the Congo Craton. The related rifting started at ca. 880 Ma (Porada and Berhorst 2000 and references therein), and first mafic intrusions within the thinned lower crust are documented to have occurred ca. 870 Ma (Müller 2002). Porada and Berhorst (2000) postulated the opening and closure of an ocean basin to explain the deposits of passive margin sediment sequences and following thrust transport (>150-km distance). In addition, geochemical and geochronological data of eclogites and gabbros of central Zambia are evidence for a Neoproterozoic ocean basin. The low geothermal gradient during eclogite facies metamorphism indicates that this basin was relatively large (John et al. 2003). These models are in contrast to the model of Dirks and Sithole (1999), who proposed that the major collisional event in the Zambezi Belt occurred between 1100–945 Ma (during Rodinia consolidation), and was followed by an extensional event at around 800 Ma (reworking of the Zambezi Belt during Rodinia break up). In this

model a nonoceanic basin closed without significant crustal thickening between 550–500 Ma.

The cooling ages of ca. 490 ± 5 Ma for muscovite and ca. 470 ± 5 Ma for biotite, determined for the Lufilian Arc, are in agreement with the results of Cosi et al. (1992), who reported Rb-Sr muscovite ages from 510 to 450 Ma (see discussion in Porada and Berhorst 2000). Cooling at a rate of 6°–7°C/Ma for the Lufilian Arc is similar to the cooling history of parts of the Zambezi Belt that record rates between 4° and 16°C/Ma (Goscombe et al. 2000 and references therein), pointing to a synchronous posttectonic evolution.

Conclusions

Combining the results of this study with the data and interpretations from the literature leads to the following model for the Pan-African mobile belts of central southern Africa (fig. 1).

Extension. *Figure 11*a. Initial rifting started at ca. 880–870 Ma on the southern edge of the Congo craton and is related to the dispersal of Rodinia. During the proceeding rifting, a passive continental margin developed (Porada and Berhorst 2000) and an ocean basin formed (John et al. 2003).

Convergence. *Figure 11*b. The geodynamic setting changed from extension to compression, and due to the convergence of the Congo and Kalahari cratons, oceanic lithosphere was subducted and eclogites were formed at ca. 600 Ma (John et al. 2003).

Collision. *Figure 11*c. After the oceanic crust was consumed, the Kalahari craton started to override the passive continental margin and collided in the final stage of the continent-continent collision with the Congo craton at ca. 530 Ma. Hence, the formation of the talc-kyanite (whiteschist) assemblages occurred during this continental collision, and the metasomatic process responsible for the whiteschist formation might be related to fluids from shallow water sediments of the overridden plate.

Cooling. *Figure 11*d. When the final collision with thrusting over a distance of >150 km (Porada and Berhorst 2000) came to an end, rapid erosion and/or tectonic uplift and finally cooling followed.

It is shown by this study that the whiteschists within the Lufilian Arc–Zambezi Belt formed under high-pressure amphibolite facies conditions. Evidence for eclogite facies metamorphism was not found in whiteschists, and the eclogites of the central Zambezi Belt were formed at ca. 600 Ma, thus the high-*P* metamorphism at ca. 530 Ma was most likely linked to a continental collision rather than to subduction zone processes. The proposed crustal thickening event affected the entire Lufilian Arc–Zambezi Belt almost simultaneously ca. 70 m.yr. after the subduction of an ocean basin. Consequently, it is suggest that the Lufilian Arc–Zambezi Belt represent part of the collisional plate boundary between the Congo and the Kalahari craton during Gondwana growth as it was initially proposed by Coward and Daly (1984).

ACKNOWLEDGMENTS

The Deutsche Forschungsgemeinschaft funded this research through grant Sche 265–10/1and 10/2. We thank P. Appel, H. Baier, H. Porada, and E. Scherer for their help and discussions and the University of Zambia and the Geological Survey of Zambia for support during fieldwork. We are grateful to the two anonymous reviewers for their constructive reviews of the manuscript.

REFERENCES CITED

Andersen, L. S., and Unrug, R. 1984. Geodynamic evolution of the Bangweulu Block, northern Zambia. Precambrian Res. 25:187–212.

Barr, M. W. C. 1997. Geology of the Chongwe River area: explanation of degree sheet 1529, SW quarter. Rep. Geol. Surv. Zambia, no. 45.

Bingen, B.; Demaiffe, D.; and Hertogen, J. 1996. Redistribution of rare earth elements, thorium, and uranium over accessory minerals in the course of amphibolite to granulite facies metamorphism: the role of apatite and monazite in orthogneisses from southwestern Norway. Geochim. Cosmochim. Acta 60: 1341–1354.

Cahen, L.; Snelling, N. J.; Delhal, J.; and Vail, J. R. 1984. The geochronology and evolution of Africa. Oxford, Clarendon.

Chopin, C. 1984. Coesite and pure pyrope in high-grade blueschists of the Western Alps: a first record and some consequences. Contrib. Mineral. Petrol. 86:107–118.

Condie, K. C. 2002. The supercontinent cycle: are there two patterns of cyclicity? J. Afr. Earth Sci. 35:179–183.

Cosi, M.; De Bonis, A.; Gosso, G.; Hunziker, J.; Martinotti, G.; Moratto, S.; Robert, J. P.; et al. 1992. Late Proterozoic thrust tectonics, high-pressure metamorphism and uranium mineralization in the Domes area,

Lufilian Arc, northwest Zambia. Precamb. Res. 58: 215–240.

Coward, M. P., and Daly, M. C. 1984. Crustal lineaments and shear zones in Africa: their relationships to plate movements. Precambrian Res. 24:27–45.

Dalziel, I. W. D. 1992. On the organisation of American plates in the Neoproterozoic and the breakout of Laurentia. GSA (Geol. Soc. Am.) Today 2:240–241.

Dirks, P. H. G. M.; Jelsma, H. A.; Vinyu, M.; and Munyanyiwa, H. 1998. The structural history of the Zambezi Belt in northeast Zimbabwe: evidence for crustal extension during the early Pan-African. S. Afr. J. Geol. 101:1–16.

Dirks, P. H. G. M., and Sithole, T. A. 1999. Eclogites in the Makuti gneisses of Zimbabwe: implications for the tectonic evolution of the Zambezi Belt in southern Africa. J. Metamorph. Geol. 17:593–612.

Dodson, M. H. 1979. Theory of cooling ages. *In* Jäger, E., and Hunziker, J. C., eds. Lectures in isotope geology. Berlin, Springer, p. 194–202.

Goscombe, B.; Armstrong, R.; and Barton, J. M. 1998. Tectonometamorphic evolution of the Chewore Inliers: partial re-equilibration of high-grade basement during the Pan-African Orogeny. J. Petrol. 39:1347–1384.

———. 2000. Geology of the Chewore Inliers, Zimbabwe: constraining the Mesoproterozoic to Palaeozoic evolution of the Zambezi Belt. J. Afr. Earth Sci. 30:589–627.

Graham, C. M., and Powell, R. 1984. A garnet-hornblende geothermometer: calibration, testing and application to the Pelona Schist, Southern California. J. Metamorph. Petrol. 2:13–21.

Hanson, G. N., and Gast, P. W. 1967. Kinetic studies in contact metamorphic zones. Geochem. Cosmochim. Acta 31:1119–1153.

Hanson, R. E; Hargrove, U. S.; Martin, M. W.; Bowring, S. A.; Krol, M. A.; Hodges, K. V.; Munyanyiwa, H.; and Blenkiskop, T. G. 1998. New geochronological constraints on the tectonic evolution of the Pan-African Zambezi Belt, south central Africa. J. Afr. Earth Sci. 18:104–105.

Hanson, R. E.; Wilson, T. J.; Brueckner, H. K.; Onstott, T. C.; Wardlaw, M. S.; Johns, C. C.; and Hardcastle, K. C. 1988. Reconnaissance geochronology, tectonothermal evolution, and regional significance of the middle Proterozoic Chonma-Kalomo Block, southern Zambia. Precambrian Res. 42:39–61.

Hanson, R. E.; Wilson, T. J.; and Munyanyiwa, H. 1994. Geologic evolution of the late Proterozoic Zambezi Belt in Zambia. J. Afr. Earth Sci. 18:135–150.

Hodges, K. V., and Crowley, P. D. 1985. Error estimation and empirical geothermobarometry for pelitic systems. Am. Mineral. 70:702–709.

Hoisch, T. D. 1990. Empirical calibration of six geobarometers for the mineral assemblage quartz + muscovite + biotite + plagioclase + garnet. Contrib. Mineral. Petrol. 104:225–234.

Holdaway, M. J. 1971. Stability of andalusite and the aluminium silicate phase diagram. Am. J. Sci. 271:97–131.

John, T.; Schenk, V.; Haase, K.; Scherer, E.; and Tembo, F. 2003. Evidence for a Neoproterozoic ocean in south central Africa from MORB-type geochemical signatures and P-T estimates of Zambian eclogites. Geology 31:243–246.

Johnson, R. L., and Vail, J. R. 1965. The junction between the Mozambique and Zambezi orogenic belts, northeast Southern Rhodesia. Geol. Mag. 101:489–495.

Johnson, S. P., and Oliver, G. J. H. 1998. A second natural occurrence of yoderite. J. Metamorph. Geol. 16:809–818.

———. 2002. High fO_2 metasomatism during whiteschist metamorphism, Zambezi Belt, Northern Zimbabwe. J. Petrol. 43:271–290.

Key, R. M.; Liyungu, A. K.; Njamu, F. M.; Somwe, V.; Banda, J.; Mosley, P. N.; and Armstrong, R. A. 2001. The western arm of the Lufilian Arc in NW Zambia and its potential for copper mineralization. J. Afr. Earth Sci. 33:503–528.

Kleemann, U., and Reinhardt, J. 1994. Garnet-biotite thermometry revisited: the effect of Al^{VI} and Ti in biotite. Eur. J. Mineral. 6:925–941.

Köppel, V. 1974. Isotopic U-Pb ages of monazite and zircon from the crust-mantle transition and adjacent units of the Ivrea and Ceneri zones (Southern Alps, Italy). Contrib. Mineral. Petrol. 43:55–70.

Koziol, A. M. 1989. Recalibration of the garnet-plagioclase-Al_2SiO_5-quartz geobarometer. EOS, Trans. Am. Geophys. Union 70:493.

Kretz, R. 1983. Symbols for rock-forming minerals. Am. Mineral. 68:277–279.

Krogh, T. E. 1982. Improved accuracy of U-Pb zircon dating by the creation of more concordant systems using an air abrasion technique. Geochim. Cosmochim. Acta 46:637–649.

Loris, N. B. T.; Chralet, J.-M.; Pechmann, E.; Clare, C.; Chabu, M.; and Quinif, Y. 1997. Caractéristiques minéralogiques, critallographiques, physico-chimiques et ages des minéralisations uranifères de Lwiswishi (Shaba, Zaire). Proc. Int. Cornet Symp., Mons R. Acad. Oversea Sci., p. 285–306.

Massonne, H.-J. 1989. The upper thermal stability of chlorite + quartz: an experimental study in the system MgO-Al_2O_3-SiO_2-H_2O. J. Metamorph. Geol. 7: 567–581.

———. 1995. Experimental and petrogenetic study of UHPM. *In* Coleman, R. G., and Wang, X., eds. Ultrahigh pressure metamorphism. Cambridge, Cambridge University Press.

Mezger, K. 1990. Geochronology in granulites. *In* Vielzeuf, D., and Vidal, P. H., eds. Granulites and crustal evolution. Dordrecht, Kluwer.

Mezger, K., and Krogstad, E. J. 1997. Interpretation of discordant U-Pb zircon ages: an evaluation. J. Metamorph. Geol. 15:127–140.

Müller, M. A. 2002. Pan-African emplacement and granulite-facies metamorphism in the Mavuradonha

Mountains, Zambezi Belt, NE Zimbabwe. Dissertation, Mainz.

Parrish, R. R. 1990. U-Pb dating of monazite and its application to geological problems. Can. J. Earth Sci. 27: 1431–1450.

Pawlig, S., and Baumgartner, L. P. 2001. Geochemistry of a talc-kyanite-chloritoid shear zone within the Monte Rosa granite, Val d' Ayas, Italy. Schweiz. Mineral. Petrogr. Mitt. 81:329–346.

Porada, H. 1989. Pan-African rifting and orogenesis in southern to Equatorial Africa and Eastern Brazil. Precambrian Res. 44:103–136.

Porada, H., and Berhorst, V. 2000. Towards a new understanding of the Neoproterozoic–Early Palaeozoic Lufilian and northern Zambezi Belts in Zambia and the Democratic Republic of Congo. J. Afr. Earth Sci. 30:727–771.

Powell, R., and Holland, T. J. B. 1988. An internally consistent thermodynamic dataset with uncertainties and correlations. 3. Applications to geobarometry, worked examples and a computer program. J. Metamorph. Geol. 6:173–204.

Rainaud, C.; Armstrong, R. A.; Master, S.; and Robb, L. J. 1999. A fertile Palaeoproterozoic magmatic arc beneath the Central African Copperbelt. *In* C. J. Stanley, ed. Mineral deposits: processes to processing. Proc. 5th SGA Meet. 10th IAGOD Symp., London, Balkema, p. 1427–1430.

Schärer, U. 1984. The effect of initial ^{230}Th disequilibrium on young U-Pb ages: the Makalu case, Himalaya. Earth Planet. Sci. Lett. 67:191–204.

Schenk, V. 1980. U-Pb and Rb-Sr radiometric dates and their correlation with metamorphic events in the granulite-facies basement of the Serre, southern Calabria (Italy). Contrib. Mineral. Petrol. 73:23–38.

Schreyer, W. 1973. Whiteschist: a high-pressure rock and its geological significance. J. Geol. 81:735–739.

———. 1977. Whiteschists: their compositions and pressure-temperature regimes based on experimental, field, and petrographic evidence. Tectonophysics 43: 127–144.

Schreyer, W., and Abraham, K. 1976. Three-stage metamorphic history of a whiteschist from Sar e Sang, Afghanistan, as part of a former evaporite deposit. Contrib. Mineral. Petrol. 59:111–130.

Schreyer, W., and Seifert, F. 1969. Compatibility relations of the aluminum silicates in the system MgO-Al_2O_3-SiO_2-H_2O and K_2O-MgO-Al_2O_3-SiO_2-H_2O at high pressures. Am. J. Sci. 267:371–388.

Schumacher, J. C., and Robinson, P. 1987. Mineral chemistry and metasomatic growth of aluminous enclaves in gedrite-cordierite-gneiss from southwestern New Hampshire, USA. J. Petrol. 28:1033–1073.

Sikatali, C.; Legg, C. A.; Bwalya, J. J.; and Ng'ambi, O. 1994. Geological and mineral occurrence map. Geol. Surv. Zambia, scale 1 : 2,000,000.

Smith, H. A., and Barreiro, B. 1990. Monazite U-Pb dating of staurolite grade metamorphism in pelitic schists. Contrib. Mineral. Petrol. 105:602–615.

Spear, F. S., and Cheney, J. T. 1989. A petrogenetic grid for pelitic schists in the system SiO_2-Al_2O_3-FeO-MgO-K_2O-H_2O. Contrib. Mineral. Petrol. 101:149–164.

Spear, F. S., and Parrish, R. R. 1996. Petrology and cooling rates of the Valhalla complex, British Columbia. Can. J. Petrol. 37:733–765.

Spear, F. S., and Rumble, D., III. 1986. Pressure, temperature, and structural evolution of the Orfordville Belt, west-central New Hampshire. J. Petrol. 27:1071–1093.

Tembo, F.; Kampunzu, A. B.; and Porada, H. 1999. Tholeiitic magmatism associated with continental rifting in the Lufilian Fold Belt of Zambia. J. Afr. Earth Sci. 28:403–425.

Thieme, J. G., and Johnson, R. L. 1977. Republic of Zambia, geological map. Sheet NW. Geol. Surv. Zambia, scale 1 : 1,000,000.

Tomascak, P. B.; Krogstad, E. J.; and Walker, R. J. 1996. U-Pb monazite geochronology of granitic rocks from Maine: implications for late Paleozoic tectonics in the Northern Appalachians. J. Geol. 104:185–195.

Unrug, R. 1996. The assembly of Gondwanaland. Scientific results of IGCP Project 288: Gondwanaland sutures and mobile belts. Episodes 19:11–20.

Vinyu, M. L.; Hanson, R. E.; Martin, M. W.; Bowring, S. A.; Jelsma, H. A.; Krol, M. A.; and Dirks, P. H. G. M. 1999. U-Pb and ^{40}Ar/^{39}Ar geochronological constraints on the tectonic evolution of the easternmost part of the Zambezi orogenic belt, northeast Zimbabwe. Precambrian Res. 98:67–82.

Vrána, S., and Barr, W. C. 1972. Talc-kyanite-quartz schists and other high-pressure assemblages from Zambia. Mineral. Mag. 38:837–846.